



**HAL**  
open science

## Highly Efficient Infrared Quantum Cutting in Tb<sup>3+</sup>– Yb<sup>3+</sup> Codoped Silicon Oxynitride for Solar Cell Applications

Yong-Tao An, Christophe Labbé, Julien Cardin, Magali Noelle Valerie Morales, Fabrice Gourbilleau

► **To cite this version:**

Yong-Tao An, Christophe Labbé, Julien Cardin, Magali Noelle Valerie Morales, Fabrice Gourbilleau. Highly Efficient Infrared Quantum Cutting in Tb<sup>3+</sup>– Yb<sup>3+</sup> Codoped Silicon Oxynitride for Solar Cell Applications. *Advanced Optical Materials*, 2013, 1 (11), pp.855–862. <10.1002/adom.201300186>. <hal-01138682>

**HAL Id: hal-01138682**

**<https://hal.science/hal-01138682v1>**

Submitted on 3 Apr 2017

HAL is a multi-disciplinary open access archive for the deposit and dissemination of scientific research documents, whether they are published or not. The documents may come from teaching and research institutions in France or abroad, or from public or private research centers.

L'archive ouverte pluridisciplinaire HAL, est destinée au dépôt et à la diffusion de documents scientifiques de niveau recherche, publiés ou non, émanant des établissements d'enseignement et de recherche français ou étrangers, des laboratoires publics ou privés.



HAL Authorization

# Highly Efficient Infrared Quantum Cutting in Tb<sup>3+</sup>–Yb<sup>3+</sup> Codoped Silicon Oxynitride for Solar Cell Applications

Yong-Tao An, Christophe Labbé,\* Julien Cardin, Magali Morales, and Fabrice Gourbilleau

**A high efficiency infrared quantum cutting effect in a Tb<sup>3+</sup>–Yb<sup>3+</sup> codoped silicon oxynitride system is demonstrated. The thin films are deposited on Si substrates by reactive magnetron co-sputtering of a Si target topped with Tb<sub>4</sub>O<sub>7</sub> and Yb<sub>2</sub>O<sub>3</sub> chips under pure nitrogen plasma. The photoluminescence dynamics are investigated, revealing a quantum efficiency of this system at 980 nm up to 197% for the higher Yb<sup>3+</sup> concentration. Thus, via a cooperative transfer mechanism between Tb<sup>3+</sup> and Yb<sup>3+</sup>, an absorbed UV–visible photon gives rise to almost two emitted IR photons. Such a down-conversion effect is demonstrated upon indirect excitation of energy donors, via defect states in the host matrix. These down-converter films could be directly and easily integrated on top of the Si-based solar cell to improve the photoelectric conversion efficiency at a lower cost. An evaluation of the additional external quantum efficiency is deduced from this optical system and found to be almost 2%.**

## 1. Introduction

Among the different approaches to improve the solar cells efficiency, the quantum cutting (QC) is one of the interesting ways proposed since the thermalization effect of the electrons is limited for the energetic photons.<sup>[1–3]</sup> Placed on top of a solar cell, a QC layer consists in dividing the absorbed UV-Visible photon energy to emit two IR photons absorbed by the classical Si solar cell below. This down-conversion (DC) process leads to a quantum efficiency ( $\eta_{QE}$ ) higher than 100% as theoretically predicted by Dexter et al.<sup>[4]</sup> and experimentally seen by different authors on Pr<sup>3+</sup>-, Tm<sup>3+</sup>-, or Gd<sup>3+</sup>-doped host matrices.<sup>[5]</sup> Almost 15 years ago, a high  $\eta_{QE}$  was achieved close to 200% by Wegh et al.<sup>[6]</sup> on a LiGdF<sub>4</sub>:Eu<sup>3+</sup>–Gd<sup>3+</sup> phosphor system. This result has relaunched the research activity on the development of efficient QC layers.<sup>[2,7,8]</sup> Another system based on double co-doping Er<sup>3+</sup>–Gd<sup>3+</sup>–Tb<sup>3+</sup> was studied in such a matrix,<sup>[9]</sup> but a system

associating a donor to Yb<sup>3+</sup> ion seems to be more promising. Indeed, the Yb<sup>3+</sup> ion has a single excited state, reducing the harmful effect of up-conversion and harvesting the energy corresponding to a photon emission of 1  $\mu$ m wavelength, just above the gap of c-Si thus limiting the thermalization.<sup>[10]</sup>

In this regard, the scientific community makes great effort to enhance the  $\eta_{QE}$  of Yb<sup>3+</sup> doped materials. The first report on efficient DC material containing Yb<sup>3+</sup> ions was on Tb<sup>3+</sup>–Yb<sup>3+</sup> system in phosphor matrix with the achievement of a 188% internal  $\eta_{QE}$ .<sup>[11]</sup> This has been followed by several studies on the same system in different host matrices such as borate ( $\eta_{QE} = 196\%$  and  $152\%$ ),<sup>[12,13]</sup> hafnia glass ceramic ( $\eta_{QE} = 138\%$ ),<sup>[14]</sup> oxyfluoride glass ( $\eta_{QE} = 120\%$  and  $166\%$ ).<sup>[15,16]</sup> High  $\eta_{QE}$  were also demonstrated in system associating Yb<sup>3+</sup> with other absorber-donor rare earth ions such as Ce<sup>3+</sup> ( $\eta_{QE} = 174\%$ ) in a borate glasses,<sup>[17]</sup> Pr<sup>3+</sup> ( $\eta_{QE} = 197\%$ ) in a fluoride,<sup>[18]</sup> and Er<sup>3+</sup> ion ( $\eta_{QE} = 196\text{--}199\%$ ) in a glass ceramic and a bromide matrix respectively.<sup>[19,20]</sup> Unfortunately, most of these rare earth-doped hosts are not easily compatible with the fabrication process of conventional crystalline silicon solar cells. Consequently, the gain achieved in terms of photon is lost by the cost required to adapt the fabrication line and/or to design a new solar cell structure. This is the reason why some investigations are now focusing on silicon integration: Zn<sub>2</sub>SiO<sub>4</sub>:Tb<sup>3+</sup>–Yb<sup>3+</sup>,<sup>[21]</sup> silicon nanocrystals,<sup>[22]</sup> Er<sup>3+</sup> in SiO<sub>2</sub>.<sup>[23]</sup>

In order to obtain both a host environment based on silicon to offer an industrial compatibility and a very high down-conversion  $\eta_{QE}$ , we propose to investigate a silicon oxynitride matrix codoped with Tb<sup>3+</sup>–Yb<sup>3+</sup> system. To perform this study, the photoluminescence (PL), PL excitation (PLE) as well as the decay lifetimes were investigated as a function of the Yb<sup>3+</sup> concentration. The latter allowed us to calculate the  $\eta_{QE}$  which has been enhanced up to almost 197% in such host matrix. By considering the non-radiative losses, a rough correction, never taken into account in previous similar studies, gives a  $\eta_{QE}$  of 183%. Our work demonstrates the feasibility of a high  $\eta_{QE}$  down-converter thin film easily deposited on a common solar cell to improve its external quantum efficiency. This additional external quantum efficiency due to this DC effect is evaluated to almost 2%.

Y.-T. An, Dr. C. Labbé, Dr. J. Cardin, Dr. M. Morales, Dr. F. Gourbilleau  
Centre de Recherche sur les Ions  
les Matériaux et la Photonique (CIMAP)  
UMR 6252 CNRS/CEA/Ensicaen/UCBN  
6 Boulevard Maréchal Juin, Cedex 4, 14050  
Caen, France  
E-mail: christophe.labbe@ensicaen.fr

**Table 1.** Atomic composition measured by RBS technique and the excess of nitrogen ( $N_{\text{excess}}$ ) deduced.

Sample name based on the $\text{Yb}_2\text{O}_3$ chip number	Si [at%]	N [at%]	O [at%]	$N_{\text{excess}}$	Tb [at%]	Yb [at%]
0Yb	32.98	46.00	20.28	14.90	0.74	0
10Yb	31.53	34.11	32.54	12.23	1.34	0.48
20Yb	30.45	38.28	27.46	12.90	1.84	1.97
30Yb	28.89	26.06	39.68	9.73	1.86	3.51

## 2. Results and Discussion

### 2.1. Samples

The thicknesses of the deposited films were measured 201 to 245 nm ( $\pm 10$  nm). The refractive index is constant of about 1.73. The concentrations of different elements deduced from the RBS experiments are displayed on the **Table 1**.

As shown, the silicon content is almost constant of about 30 at% whereas the nitrogen content tends to decrease with the  $\text{Yb}^{3+}$  concentration in favor of the oxygen element. The amount of oxygen contained only in the  $\text{Tb}_4\text{O}_7$  and  $\text{Yb}_2\text{O}_3$  chips could contribute to the formation of  $\text{SiO}_2$  phase detected by the presence of Si-O bond in FTIR spectrum as previously reported.<sup>[24]</sup> The refractive index measured is consequently the signature of a composite layer containing  $\text{SiO}_2$  ( $n = 1.55$ ) and  $\text{Si}_3\text{N}_4$  ( $n = 2.00$ ) phases. Moreover, the lower 1.73 value could also be ascribed to the excess of nitrogen incorporated with respect to the stoichiometric  $\text{Si}_3\text{N}_4$  matrix. Indeed the nitrogen excess ( $N_{\text{excess}}$ ), responsible for the deviation from a perfect  $\text{SiO}_2 + \text{Si}_3\text{N}_4$  mixture is calculated with help of the equation (1):

$$N_{\text{excess}} = \frac{[N] - (4/3)[\text{Si}] + (2/3)[\text{O}] - (7/6)[\text{Tb}] - (1/4)[\text{Yb}]}{[N] + [\text{Si}] + [\text{O}] + [\text{Tb}] + [\text{Yb}]} \quad (1)$$

where the term [element] represents the atomic concentration (at%) of the aforesaid element.<sup>[25]</sup> On the basis of Kistner et al.<sup>[26]</sup> study, this excess of nitrogen explains the value of 1.73 measured. So our deposited thin film is a nitrogen-rich silicon oxynitride (NRSON). Note that even if the number of  $\text{Tb}_4\text{O}_7$  chips is constant during the deposition run, the  $\text{Tb}^{3+}$  concentration is multiplied by 2.5 with the increasing number of the  $\text{Yb}_2\text{O}_3$  chips.

### 2.2. Photoluminescence

The PL spectrum of the  $\text{Tb}^{3+}$  monodoped sample is displayed in **Figure 1** with a 239 nm excitation wavelength, corresponding to the best PL signal taking account our experimental set up response.

In the visible range, the peaks of the  $\text{Tb}^{3+}$  at 545, 590 and 624 nm were identified as the transitions  $^5\text{D}_4 \rightarrow ^7\text{F}_j$  ( $j = 5, 4, 3$ ) respectively. In our previous study,<sup>[24]</sup> a non-resonant excitation wavelength with the  $\text{Tb}^{3+}$  ion at 325 nm, allow us to see also the transition at 490 nm, like Jeong et al. with the same matrix,<sup>[27]</sup>

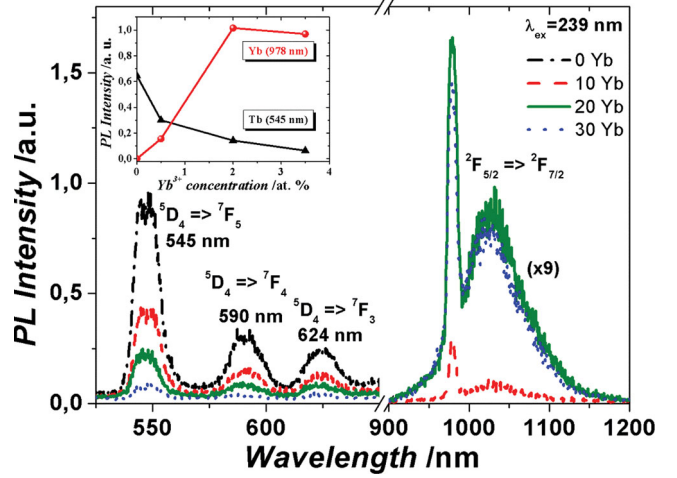


**Figure 1.** PL spectra under 239 nm excitation wavelength as a function of  $\text{Yb}^{3+}$  concentration. In inset, the variation of the  $\text{Tb}^{3+}$  and  $\text{Yb}^{3+}$  PL intensities with the  $\text{Yb}^{3+}$  concentration. Note that each  $\text{Yb}^{3+}$  intensity is multiplied by a factor of 9 for a best readability.

corresponding to the transition  $^5\text{D}_4 \rightarrow ^7\text{F}_6$ , hidden by the second-order grating with a 239 nm excitation wavelength. These four transitions are depicted in **Figure 2**.

On the **Figure 1**, when a small content of  $\text{Yb}^{3+}$  ions is added (10Yb curve), we note a remarkable decreasing  $\text{Tb}^{3+}$  PL intensity and concomitantly in the IR range emerging two typical  $\text{Yb}^{3+}$  peaks located at 976 and 1026 nm coming from  $^2\text{F}_{5/2} \rightarrow ^2\text{F}_{7/2}$  transition. The variation of these visible and IR PL peaks intensities versus the  $\text{Yb}^{3+}$  concentration are shown in the inset of **Figure 1**. The PL intensity of the  $\text{Tb}^{3+}$  ion at 545 nm decreases, with the  $\text{Yb}^{3+}$  concentration, while that of  $\text{Yb}^{3+}$  PL increases. This opposite behavior is the sign of cooperative DC energy transfer (ET) as shown on the **Figure 2**. The  $^5\text{D}_4 \rightarrow ^7\text{F}_6$   $\text{Tb}^{3+}$  energy transition (490 nm  $\approx 2.53$  eV) is divided

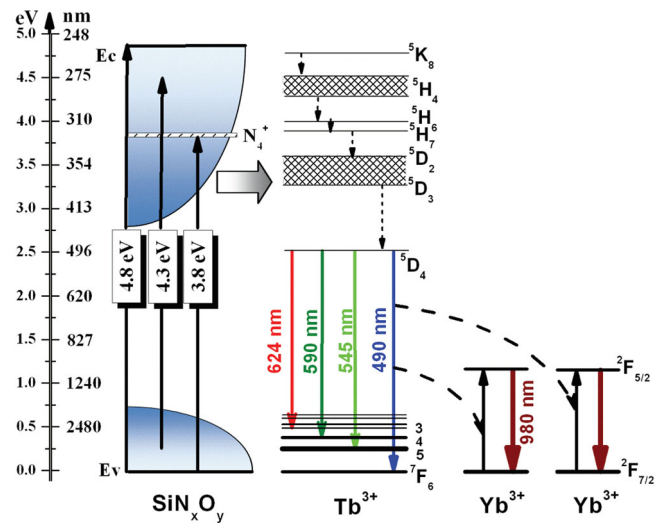


**Figure 2.** Scheme of the  $\text{Tb}^{3+}$  and  $\text{Yb}^{3+}$  energy diagram depicting the QC effect. Note that in this diagram we have supposed for the legibility that the top of the valence band ( $E_v$ ) is at the same energy than the rare earths' ground states.

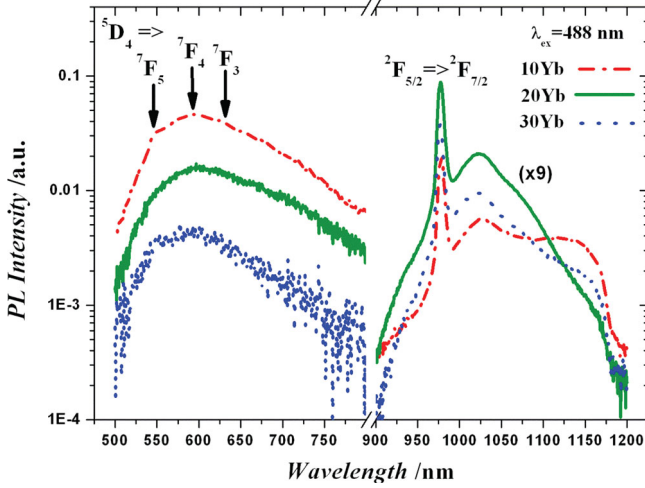


**Figure 3.** PL spectra of the codoped  $\text{Tb}^{3+}$ - $\text{Yb}^{3+}$  samples excited at 488 nm wavelength. Note that each the  $\text{Yb}^{3+}$  intensity is multiplied by a factor of 9 for a best readability.

into two IR photons coming from two  ${}^2\text{F}_{5/2}$ - ${}^2\text{F}_{7/2}$   $\text{Yb}^{3+}$  energy transitions (980 nm  $\approx$  1.26 eV).<sup>[11,28]</sup> We also observe a saturation and a slight decrease of the  $\text{Yb}^{3+}$  PL intensity for the 30Yb curve, when we almost have one  $\text{Tb}^{3+}$  ion (1.86 at%) for two  $\text{Yb}^{3+}$  ions (3.51 at%) (see Table 1). This could be the expression of the usual quenching effect observed for high concentration corresponding to a migration between the  $\text{Yb}^{3+}$  ions into non-radiative defects. But the self-quenching effect is ruled out here because it has been observed for system containing more than 10 at% concentration.<sup>[29,30]</sup> So this saturation could be explained by the beginning of the formation of  $\text{Yb}^{3+}$  clusters due to the annealing of the samples at 700 °C, reducing de facto the active numbers of  $\text{Yb}^{3+}$  ions.<sup>[31]</sup>

One may argue that, depending on the used host matrix, the 239 nm excitation wavelength (5.2 eV) could induce charge transfer energy on the Yb ion ( $\text{Yb}^{3+} \rightarrow \text{Yb}^{2+}$ ) and thus directly excite the  $\text{Yb}^{3+}$  ion without sensitizing the  $\text{Tb}^{3+}$ .<sup>[32]</sup> To avoid this drawback, we have excited the three  $\text{Yb}^{3+}$  samples at 488 nm which is clearly non resonant with the  $\text{Yb}^{3+}$  ion, but resonant with the  $\text{Tb}^{3+}$  ion.<sup>[21,29]</sup>

The Figure 3 depicts clearly the  $\text{Yb}^{3+}$  PL spectra in the IR range suggesting an ET via the  $\text{Tb}^{3+}$  ion is possible. The visible range shows this time a broad band of almost 200 nm width and centered at 600 nm. This broad emission band is attributed to the band tail states of the matrix.<sup>[24,27,33]</sup> Indeed this band tail comes from localized states associated with defects such as dangling bonds in the host matrix. Its PL spectrum is strongly blue-shifted with the decrease of the excitation wavelength (see Figure S1) due to the occupancy of the density of states. This visible band finally disappear when we use an excitation (239 nm  $\approx$  5.2 eV) higher to the band gap (4.8 eV),<sup>[24]</sup> due to the trapping of the electron (Figure 1 and drawing in Figure 2). This effect is also seen by Kistner et al.<sup>[26]</sup> but in their case the excitation wavelength is constant while the gap changes with the composition.

We also distinguish on Figure 3 a weak PL intensity of the  $\text{Tb}^{3+}$  peaks at 545, 590, and 624 nm identified as the

transitions  ${}^5\text{D}_4 \rightarrow {}^7\text{F}_j$  ( $j = 5, 4, 3$ ) respectively (Figure 2). In our previous study without Yb doping,<sup>[24]</sup> we mentioned two energy transfer mechanisms producing these four transitions coming from the  ${}^5\text{D}_4$  level of the  $\text{Tb}^{3+}$  ion: (i) one coming from the carriers across the optical gap into the extended states-carriers that could be captured directly by  $\text{Tb}^{3+}$  related states, (ii) the second when excitation energy is lower than the gap, carriers trapped in the band tail states can transfer energy to  $\text{Tb}^{3+}$  ions. So with the 488 nm (and also 457 nm and 476 nm not shown) excitation wavelength, which is non resonant with the  $\text{Yb}^{3+}$  ion, the last mechanism is involved, and gives a significant  $\text{Yb}^{3+}$  PL intensity with the help of a DC effect. The best PL intensity is again obtained for the 20Yb sample.

### 2.3. Photoluminescence Excitation

To investigate in more details the excitation range of the  $\text{Tb}^{3+}$  ion to get ET towards  $\text{Yb}^{3+}$ , we perform the PLE spectra of the samples with and without  $\text{Yb}^{3+}$  ions normalized to the thickness (Figure 4).

The PLE measurements are carried out by setting the detection at 545 nm attributed to the  ${}^5\text{D}_4 \rightarrow {}^7\text{F}_5$  transition of  $\text{Tb}^{3+}$ , also including the band tail. The PLE spectra range is extended from about 250 to 550 nm ( $\approx$  2.2–5.0 eV), corresponding to the solar spectra range available for the DC effect.<sup>[1]</sup> The PLE intensities behaviors following the lowering of the  $\text{Tb}^{3+}$  PL intensity with the  $\text{Yb}^{3+}$  content attest that the transfer mechanism involved in this system is efficient in a wide range of wavelengths. The PLE spectra comprise three peaks centered at almost 3.8 eV, 4.3 eV, and 4.8 eV. These three peaks are also identified in a sample without any rare earth (not shown) respectively centered at 3.3 eV, 3.8 eV, and 4.3 eV. The first peak at 3.3e V is identified as a nitrogen defect state ( $\text{N}_4^+$ ).<sup>[34]</sup> The second at 3.8 eV with a very broad band (almost 1.5 eV width) is linked to the band tail,<sup>[35]</sup> while the third one at 4.3 eV is due to the gap of the NRSON host matrix. Indeed the refractive index of the undoped sample is found to be 1.80 corresponding to a tauc gap of 4.3 eV based

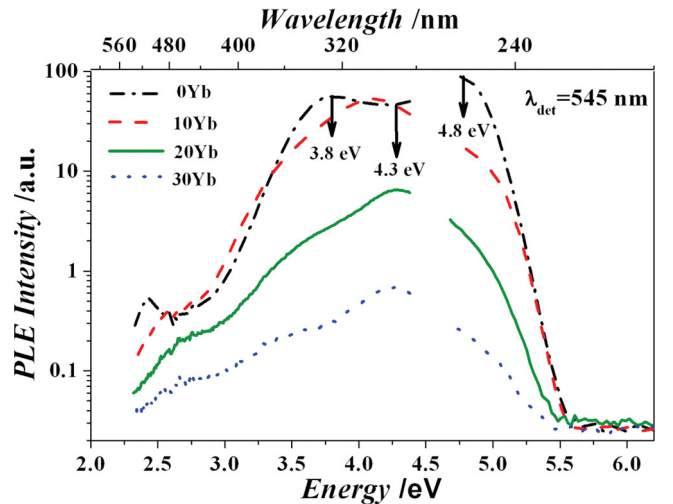


**Figure 4.** PLE spectra detected at a 545 nm wavelength corresponding to the  ${}^5\text{D}_4 \rightarrow {}^7\text{F}_5$  transition of  $\text{Tb}^{3+}$  for three different  $\text{Yb}^{3+}$  concentrations.

to the average results reported by Kistner et al.<sup>[26]</sup> and Wang et al.<sup>[36]</sup> The four rare earth-doped samples in this study have a refractive index of 1.73 resulting in a slightly higher gap which explains the energy position shift of almost 0.5 eV of their three peaks compared to their undoped counterparts. Therefore the three peaks at 3.8 eV, 4.3 eV, and 4.8 eV of the doped samples on the Figure 4, are attributed also to the nitrogen defect state ( $N_4^+$ ), band tail and band gap respectively, and are represented schematically in the diagram of Figure 2. The excitation of  $Tb^{3+}$  in such thin films was previously studied and has proved the involvement of these energy states in the excitation mechanism, confirming our results of the PLE spectra.<sup>[27,35]</sup> Thus the excitation of the  $Tb^{3+}$  ions in a large spectral range in order to obtain a DC effect with an  $Yb^{3+}$  ion is possible, upon indirect excitation of energy donors, via defect states in the NRSON host matrix.

## 2.4. Time-Resolved Photoluminescence

Figure 5 depicts the decay times of the  $Tb^{3+}$  at 545 nm ( $^5D_4 \rightarrow ^7F_5$ ) under 239 nm excitation wavelength with different concentrations of  $Yb^{3+}$ .

The lifetime curves present a biexponential decay. For example, the  $Yb^{3+}$ -free sample displays fast (151  $\mu s$ ) and slow (627  $\mu s$ ) components. Note that the lifetime linked to the band tail is a nanosecond time scale and is not detectable here.<sup>[36,37]</sup> The slow decay value is comparable to that obtained in similar matrix with a  $Tb^{3+}$  concentration four times lower.<sup>[27]</sup> These two decays could correspond to the  $Tb^{3+}$  ions linked to the  $Tb$  cluster (fast component) and the "isolated"  $Tb$  ions (slow component).<sup>[38]</sup> To overcome such non exponential decays, a mean decay time ( $\tau_m$ ) is calculated by the formula (2):

$$\tau_m = \int_0^{\infty} \left( \frac{I(t)}{I_0} \right) dt \quad (2)$$

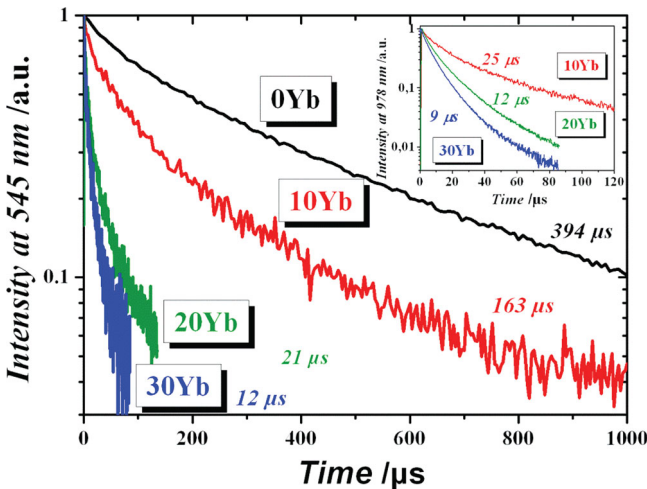


Figure 5.  $Tb^{3+}$  decay times at 545 nm under a 239 nm excitation wavelength with different concentrations of  $Yb^{3+}$ . In inset:  $Yb^{3+}$  decay times at 980 nm under a 239 nm excitation wavelength with different concentrations of  $Yb^{3+}$ .

where  $I(t)$  is the decay intensity and  $I_0$  the maximum of the  $I(t)$ .<sup>[39]</sup> The values of the different samples are presented on Figure 5. The  $\tau_m$  of the  $Tb^{3+}$  falls down drastically with the increase of the  $Yb^{3+}$  concentrations showing a reduction by a factor of more than 30. Such an evolution with the  $Yb^{3+}$  concentration was also observed in previous studies,<sup>[3,13,15,16,21,29,40]</sup> but in a lower proportion of a factor 4 at maximum whatever the  $Yb^{3+}$  concentration. The decrease was identified as the consequence of the cooperative ET from one  $Tb^{3+}$  to two  $Yb^{3+}$  ions acting as quantum cutting mechanism, and the factor 30 presuppose a very high efficiency transfer.

## 2.5. Quantum Efficiency

To quantify such cooperative ET, we calculate the energy transfer efficiency ( $\eta_{ETE}$ ) at 545 nm ( $^5D_4 \rightarrow ^7F_5$ ) described in the formula (3):

$$\eta_{ETE} = 1 - \frac{\tau_{Tb-Yb}}{\tau_{Tb}} \quad (3)$$

where  $\tau_{Tb-Yb}$  and  $\tau_{Tb}$  are the decay times of the  $Tb^{3+}$  with and without  $Yb^{3+}$ , respectively. Thus the quantum efficiency ( $\eta_{QE}$ ) usually defined as the ratio between the total number of emitted photons and the total number of absorbed photons, is described by the formula (4):

$$\eta_{QE} = \eta_{Tb} (1 - \eta_{ETE}) + 2\eta_{ETE} = 2 - \frac{\tau_{Tb-Yb}}{\tau_{Tb}} \quad (4)$$

assuming that the quantum efficiency of  $Tb^{3+}$  is 1.<sup>[6,11]</sup>

The Figure 6 shows the  $\eta_{QE}$  of the transfer according to the  $Yb^{3+}$  concentration. To calculate the  $\eta_{QE}$ , it is always supposed implicitly that  $\tau_{Tb}$  is constant in order to compare the different  $Yb^{3+}$  concentrations. During the increase of the  $Yb^{3+}$  concentration, we note an increase of the  $Tb^{3+}$  content by a factor of 2.5, from 0.74 at% to 1.86 at%, mentioned previously in the Table 1, although the number of the  $Tb^{3+}$  chips is kept constant during the deposition process. This increase of the  $Tb^{3+}$  concentration could contribute to a variation of its own lifetime by two different effects (cross relaxation or

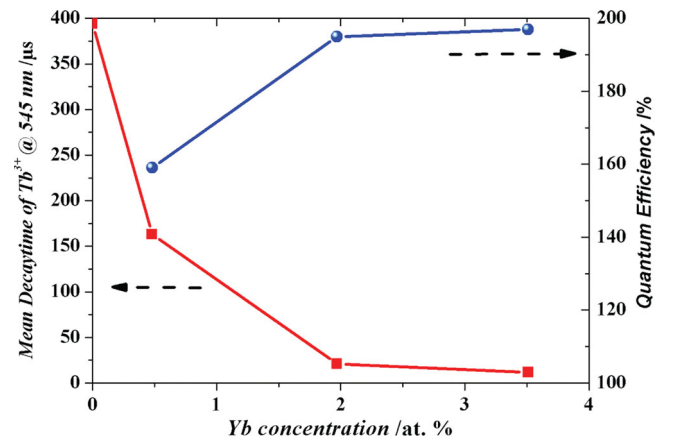


Figure 6.  $Tb^{3+}$  decay times at 545 nm under a 239 nm excitation wavelength with different concentrations of  $Yb^{3+}$ .

migration) and affect the comparison. In the first effect, the known cross relaxation is defined by ( ${}^5D_3 \rightarrow {}^5D_4$ )/( ${}^7F_6 \rightarrow {}^7F_0$ ) transitions, which contributes to extend the  ${}^5D_4$  experimental lifetime and consequently underestimates the  $\eta_{QE}$  obtained.<sup>[41]</sup> On the contrary, the self-quenching process, caused by the migration of the excitation energy of the  $Tb^{3+}$  to non-radiative defects could reduce the  $\tau_{Tb}({}^5D_4)$  and overestimate the  $\eta_{QE}$ . But the decrease of the intensity linked to the migration is usually observed for very high concentration of  $Tb^{3+}$ , which has not been studied in this work.<sup>[42]</sup> So the  $\tau_{Tb}({}^5D_4)$  is not affected by  $Tb^{3+}$  concentration used. On Figure 6, we observe an increasing of the  $\eta_{QE}$  following by a plateau at 197%. This plateau is due to weak variation of the  $\tau_{Tb-Yb}$  values (21  $\mu s$  to 12  $\mu s$ ) compare to the  $\tau_{Tb}$  (394  $\mu s$ ). Note that the behaviors of the variation with the  $Yb^{3+}$  concentration of the fast and slow  $Tb^{3+}$  decay times are the same as the  $\tau_m$ , which represents an average of these two components. So for the fast and slow components, the  $\eta_{QE}$  limits are almost the same, 198% and 195% respectively. This means that almost two  $Yb^{3+}$  ions are excited for one excited  $Tb^{3+}$  ion attesting a highly efficient quantum cutting mechanism. This limit has been approached for a  $Tb^{3+}-Yb^{3+}$  system in phosphor matrix ( $\eta_{QE} = 188\%$ )<sup>[11]</sup> or borate ( $\eta_{QE} = 196\%$ )<sup>[12]</sup> and with other rare earth with  $Yb^{3+}$  like  $Pr^{3+}$  ( $\eta_{QE} = 197\%$ )<sup>[18]</sup>, or  $Er^{3+}$  ( $\eta_{QE} = 196-199\%$ ).<sup>[19,20]</sup>

Usually, the  $\eta_{QE}$  calculations suppose that the decrease of the  $Tb^{3+}$  lifetime with the  $Yb^{3+}$  content is completely attributed to the ET.<sup>[13]</sup> But the increase of the  $Yb^{3+}$  concentration could introduce some non-radiative (NR) losses, by inclusion of defects or impurities, contributing to the fall of the decay time and overestimate the  $\eta_{QE}$ . To investigate this point, we have measured the  $Yb^{3+}$  lifetime at 980 nm wavelength (inset Figure 5). The  $Yb^{3+}$  decay time is reduced from 25  $\mu s$  to 9  $\mu s$  with the increase of the concentration, revealing the NR losses, because the self-quenching effect is not expected as mentioned above.<sup>[29]</sup> In spite of the  $Yb^{3+}$  lifetime diminution, we observe that its PL intensity is constantly increasing (inset Figure 1) with the Yb content. This is due to the growing number of excited  $Yb^{3+}$  ions and the efficient ET that counterbalances this weak decrease linked to the NR losses. To take into account this effect, and see how this decrease could affect the  $\eta_{QE}$ , we have estimated the nonradiative rate ( $1/\tau_{NR}$ ) considering that  $\tau_{Tb}$  is affected by the ET and NR losses and can be described by the following equation (5):

$$\frac{1}{\tau_{Tb-Yb}} = \frac{1}{\tau_{Tb}} + \frac{1}{\tau_{ET}} + \frac{1}{\tau_{NR}} \quad (5)$$

So we can define in equation (6), a new lifetime by  $\tau'_{Tb-Yb}$  to calculate the new quantum efficiency  $\eta'_{QE}$  taking into account the NR part.

$$\frac{1}{\tau'_{Tb-Yb}} = \frac{1}{\tau_{Tb-Yb}} - \frac{1}{\tau_{NR}} = \frac{1}{\tau_{Tb}} + \frac{1}{\tau_{ET}} \quad (6)$$

To roughly estimate the non-radiative rate ( $1/\tau_{NR}$ ) for the  $Tb^{3+}$ , we use the  $Yb^{3+}$  decay measurements considering that the lowering of the quality approximately affects the decay times of the rare earth in the same proportion (see inset Figure 5). Based on the fact that we assume there are no NR losses for the decay

time ( $\tau_{Yb} = 25 \mu s$ ) of the lower  $Yb^{3+}$  concentration sample, the non-radiative rate is described by the equation (7):

$$\frac{1}{\tau_{NR}} = \frac{1}{\tau_{Yb}} - \frac{1}{\tau'_{Yb}} \quad (7)$$

where  $\tau'_{Yb}$  is the decay time of the higher  $Yb^{3+}$  concentration sample (9  $\mu s$ ). The  $\tau'_{Tb-Yb}$  is found to be almost 66  $\mu s$ , then giving a new quantum efficiency  $\eta'_{QE}$  of 183%, compared to the 197% found, without taking into account these NR losses. Of course the component  $1/\tau_{NR}$  is not exactly the same for  $Tb^{3+}$  and  $Yb^{3+}$ , but this method could give a rapid proportion of the overestimated  $\eta_{QE}$ , never made in the literature.

### 3. Additional External Quantum Efficiency Evaluation

The additional external quantum efficiency ( $\eta_{EQE}^{add}$ ) induced by this DC layer has been estimated. An external quantum efficiency of a conventional solar cell ( $sc$ ) with a DC film is noted  $\eta_{EQE}^{with}$ . To extract the additional external quantum efficiency cause by the DC layer, we have to take into account a possible loss of the external quantum efficiency ( $\eta_{EQE}^{loss}$ ) of the  $sc$  due to its partial occultation by this converting frequency layer. Then the additional external quantum efficiency ( $\eta_{EQE}^{add}$ ) can thus be obtained in according to the equation (8):

$$\eta_{EQE}^{add} = \eta_{EQE}^{with} - \eta_{EQE}^{loss} \quad (8)$$

The  $\eta_{EQE}^{with}$  is defined by the ratio between the charge carriers generated by the  $sc$  and the incident photons on the  $sc$  in the DC wavelength range ( $\phi_{sun}$ ), i.e. ,between 250 nm and 550 nm as mentioned above.<sup>[1]</sup> The efficiency of the  $sc$  for a corresponding wavelength  $\lambda$  is called ( $\eta_{sc}^{\lambda}$ ). Thus the charge carriers generated by the  $sc$  are obtained by the product of the  $\eta_{sc}^{980}$  and the incident photons flux on the  $sc$  at 980 nm wavelength coming from the conversion performed by the DC layer ( $\phi'_{sc}$ ). The  $\eta_{EQE}^{with}$  is well defined by the equation (9):

$$\eta_{EQE}^{with} = \eta_{sc}^{980} \frac{\phi'_{sc}}{\phi_{sun}} \quad (9)$$

To separate each efficiency, corresponding at each step of the conversion, we define  $\Delta\phi_{DC}$  representing the absorbed photon flux inside the DC layer. After the DC process,  $\phi'_{DC}$  describes the emitted photon flux at the 980 nm wavelength inside the DC layer (Figure 7).

Therefore the  $\eta_{EQE}^{with}$  can be rewritten by the equations (10) and (11):

$$\eta_{EQE}^{with} = \eta_{sc}^{980} \left( \frac{\phi_{DC}}{\phi_{sun}} \right) \left( \frac{\phi'_{DC}}{\phi_{DC}} \right) \left( \frac{\phi'_{sc}}{\phi'_{DC}} \right) \quad (10)$$

$$\eta_{EQE}^{with} = \eta_{sc}^{980} \cdot \eta_{abs}^{DC} \cdot \eta_{conv}^{DC \rightarrow 980} \cdot \eta_{extrac}^{980} \quad (11)$$

where,  $\eta_{abs}^{DC}$ ,  $\eta_{conv}^{DC \rightarrow 980}$ , and  $\eta_{extrac}^{980}$  are the different efficiencies linked respectively to the different terms of the equation (10).

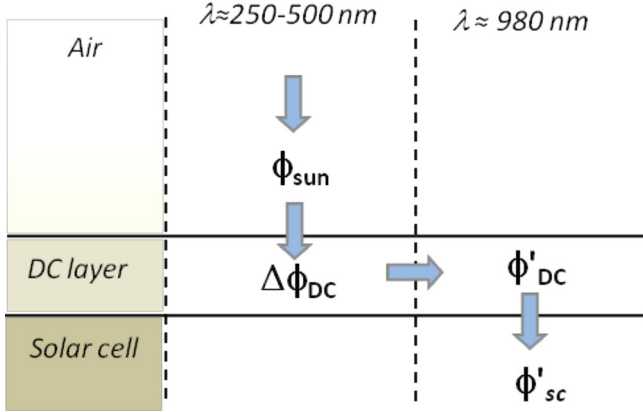


Figure 7. Schematic diagram of the down-converter system.

These four efficiencies can be estimated using the following approach:

i. The efficiency  $\eta_{sc}^{980}$

This efficiency can be obtained at 980 nm (1.26 eV) using the efficiency versus band gap calculated for the AM1.5G spectra in the extended Shockley–Queisser approach.<sup>[43]</sup> At 980 nm, the  $\eta_{sc}^{980}$  is found to be equal to 32.9%.

ii. The efficiency  $\eta_{abs}^{DC}$

Coming from the ellipsometry measurement at each wavelength, the absorption coefficient spectrum of the host matrix is determined using the imaginary part of the refractive index. This spectrum is used with the help of the solar spectral irradiance AM1.5G (equal to  $\phi_{sun}$  at each DC range wavelength) to calculate the transmitted photon flux after the DC layer ( $\phi_{after DC}$ ) at the normal incident angle (Figure 8).

The integrated photon flux of  $\phi_{sun}$  on the spectral range is equal to  $6.05 \times 10^{12}$  ph s<sup>-1</sup> m<sup>-2</sup> while the integrated photon flux of  $\phi_{after DC}$  is equal to  $5.20 \times 10^{12}$  ph s<sup>-1</sup> m<sup>-2</sup>. The number of absorbed photons in the DC layer is then equal to 0.85 ×

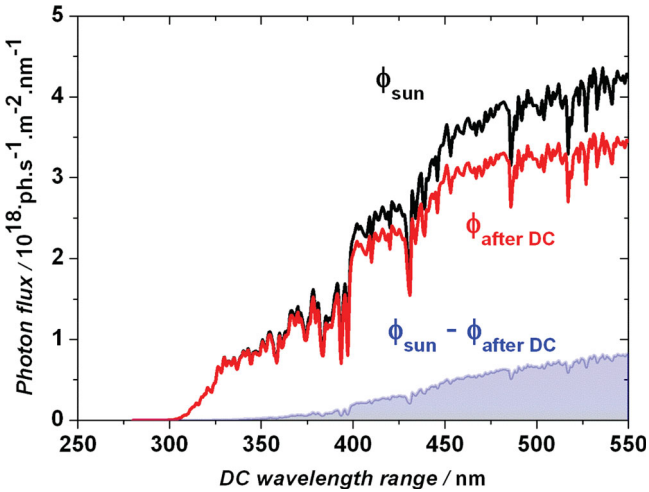


Figure 8. Photon flux of the solar spectral irradiance AM1.5G on the DC range ( $\phi_{sun}$ ), transmitted photon flux after the DC layer ( $\phi_{after DC}$ ), and the photon flux absorbed by the DC layer ( $\Delta\phi_{DC} = \phi_{sun} - \phi_{after DC}$ )

$10^{12}$  ph s<sup>-1</sup> m<sup>-2</sup>. Consequently, the  $\eta_{abs}^{DC}$  is equal to 14% of the incident solar photons, on the DC range.

iii. The efficiency  $\eta_{conv}^{DC \rightarrow 980}$

The energy transfer demonstrated above between the host matrix and the Tb<sup>3+</sup> ion ( $\eta_{matrix \rightarrow Tb}$ ) is supposed here equal to 100%. It means that all the absorbed photons by the host matrix are transferred to the Tb<sup>3+</sup> ion and contributed to the DC conversion process. Note that the photon flux is less than the common densities of the rare earth ions usually used and consequently the efficiency is not limited by an eventual saturation. So the  $\eta_{conv}^{DC \rightarrow 980}$  efficiency is defined by the product of ( $\eta_{matrix \rightarrow Tb} = 100\%$ ) and the  $\eta_{QE}$  found in Section 2.5 at 183% taking account the NR losses, i.e., a  $\eta_{conv}^{DC \rightarrow 980}$  equal to 183%.

iv. The efficiency  $\eta_{extrac}^{980}$

The PL emission is omnidirectional. So, in this part, we have to take into account the extraction of the down-converted low-energy photons in the sc which are confined in a layered media formed by the DC layer stack on the sc.<sup>[7]</sup> Based on a transfer matrix formalism and electric dipole source terms,<sup>[44]</sup> a method of modeling light emission in layered media has been developed. This method leads us to the distribution modeling of emitted intensities versus emission angle in each considered medium (Figure 9a) and versus wavelength i.e. around 980 nm for the Yb<sup>3+</sup> ion in this case. We consider an average DC layer thickness of 225 nm, with refractive index describe by a new amorphous model.<sup>[45]</sup> The emission of Yb<sup>3+</sup> ions was modeled by a Lorentzian function centered at 980nm and with a FWHM of 50nm. So we obtained the PL spectra by the integration over emission angles in DC and sc materials (Figure 9b). This numerical calculation shows that the efficiency  $\eta_{extrac}^{980}$  is equal to 30%.

Therefore the external quantum efficiency induced by the DC layer ( $\eta_{EQE}^{with}$ ) is found to be 2.53%, using the equation (12).

$$\eta_{EQE}^{with} = \eta_{sc}^{980} \cdot \eta_{abs}^{DC} \cdot \eta_{conv}^{DC \rightarrow 980} \cdot \eta_{extrac}^{980}$$

$$= 32.9\% \times 14\% \times 183\% \times 30\% = 2.53\% \quad (12)$$

To calculate the loss due to the occultation by DC layer ( $\eta_{EQE}^{loss}$ ) of 14% of the incident energy on the sc, we assume no DC effect ( $\eta_{conv}^{DC \rightarrow 980} = 100\%$ ) and full extraction ( $\eta_{extrac}^{980} = 100\%$ ) for the sc. The efficiency calculated for the AM1.5G spectra in the extended Shockley–Queisser approach,<sup>[43]</sup> gives a  $\eta_{sc}^{400}$  of 3.5%. at a 400 nm (3.1 eV) wavelength, corresponding to the middle of the DC range. Then the external quantum efficiency of the sc ( $\eta_{EQE}^{loss}$ ) is equal to 0.49% following the equation (13):

$$\eta_{EQE}^{loss} = \eta_{sc}^{400} \cdot \eta_{abs}^{DC} \cdot \eta_{conv}^{DC \rightarrow 980} \cdot \eta_{extrac}^{980}$$

$$= 3.5\% \times 14\% \times 100\% \times 100\% = 0.49\% \quad (13)$$

So using the equation (8), the additional external quantum efficiency ( $\eta_{EQE}^{add}$ ) is equal to almost 2% ( $\eta_{EQE}^{add} = 2.53 - 0.49\%$ ). It means that the stacking of a DC layer gives 2% more external quantum efficiency compare to a bare sc. However, it's interesting to calculate also the maximum  $\eta_{EQE}^{loss}$  with the  $\eta_{sc}^{550}$  (17.5%), obtained at the 550 nm (2.25 eV) giving a value of

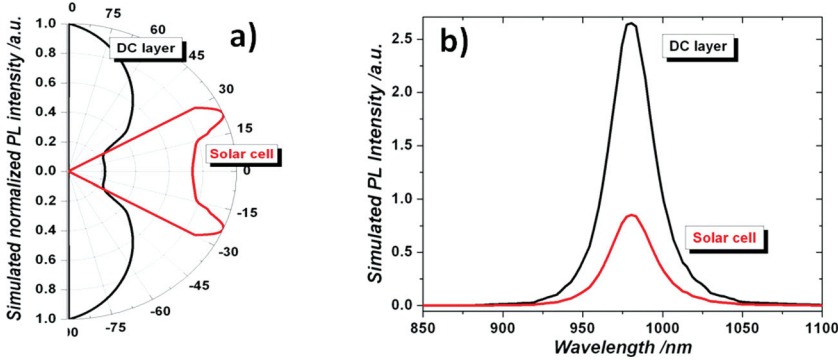


**Figure 9.** a) Emission pattern normalized of the  $\text{Yb}^{3+}$  ion emission in the DC layer (black) and in the  $sc$  (red) at a 980 nm wavelength. b) PL spectra obtained by the integration over emission angles in DC and  $sc$  material, centered at 980 nm.

2.45%. In this case the  $\eta_{\text{EQE}}^{\text{add}}$  is close to zero ( $\eta_{\text{EQE}}^{\text{add}} = 2.53\text{--}2.45\%$ ), indicating that is not interesting to use a DC layer. But on the DC range, the  $\eta_{\text{sc}}^{\text{e}}$  decreases with the wavelength witnessing the thermalization effect. So, at least the  $\eta_{\text{EQE}}^{\text{add}}$  is positive. This is the reason, why we choose the middle wavelength of the DC range to estimate additional external efficiency value of 2%.

This latter has to be compared with theoretical results obtained in the literature. Trupke et al.<sup>[7]</sup> have estimated a maximum  $\eta_{\text{EQE}}^{\text{add}}$  of about 9%, while Abrams et al.<sup>[46]</sup> found 7%. We are almost 4 times lower than these theoretical estimations. The  $\eta_{\text{EQE}}^{\text{with}}$  could however be improved, and consequently the  $\eta_{\text{EQE}}^{\text{add}}$  also, by different technical processes. Indeed, in playing in particular with the nitrogen excess, the refractive index would increase, as well as the absorption. In addition the increasing of the DC layer refractive index should increase the efficient of the  $sc$  as mentioned by Trupke et al.<sup>[7]</sup>. Furthermore, this deposit process opens the possibility of designing Bragg mirror to have a good optical confinement in playing with the excess of silicon and/or nitrogen<sup>[47]</sup> and to increase the low extraction part found to be only 30% in the  $sc$ . Such process might give some improvement of an external quantum efficiency photovoltaic cell.

## 4. Conclusion

In summary, a  $\text{Tb}^{3+}\text{--Yb}^{3+}$  codoped silicon oxynitride system was deposited on Si substrate by magnetron cosputtering for different  $\text{Yb}^{3+}$  concentrations. RBS measurements were investigated to confirm the element composition and the excess of nitrogen. PL spectra and decay times were performed to point out a cooperative energy transfer between the  $\text{Tb}^{3+}$  and the  $\text{Yb}^{3+}$ . Indeed a down-conversion effect is established upon indirect excitation of energy donors, via defect states in the host matrix. It was found this down-conversion process leads to quantum efficiency equal to 183% taking into account the nonradiative losses for the higher  $\text{Yb}^{3+}$  concentration with a rough estimation. Without taking into account these losses and in order to compare to the literature, this corresponds to a quantum efficiency of 197%, leading to almost one photon energy into two emitted IR photon energies. In addition,

these thin films are easily integrated on the top of c-Si solar cell, compatible with solar spectra range which is available for the down-conversion effect and its additional external quantum efficiency coming from this down-conversion process is estimated to almost 2%.

## 5. Experimental Section

**Samples Preparation:** The films were deposited on p-type 250  $\mu\text{m}$ -thick [001] 2 $\text{''}$  Si substrates by means of a reactive magnetron co-sputtering setup, using pure Si target topped with  $\text{Tb}_4\text{O}_7$  and  $\text{Yb}_2\text{O}_3$  chips. The deposition temperature and radio frequency power density were fixed at 200  $^\circ\text{C}$  and 1.23  $\text{W cm}^{-2}$  respectively, while the nitrogen plasma used was set at a pressure of 23  $\mu\text{bar}$ .<sup>[24]</sup> The Si target was covered with five  $\text{Tb}_4\text{O}_7$  chips and different numbers of  $\text{Yb}_2\text{O}_3$  chips going from 0, to 10, 20, or 30 in order to increase the  $\text{Yb}^{3+}$  concentration. After deposition, the samples were annealed at 700  $^\circ\text{C}$  during 1h in a conventional furnace under a dry nitrogen flow.

**Sample Composition Analysis:** The compositions of the deposited layers were determined by Rutherford backscattering spectrometry (RBS) using the 2.5 MeV Van de Graaff-type accelerator located at the Institute of NanoSciences in Paris (INSP). The RBS data were obtained using a 1.5 MeV  $^4\text{He}^+$  ions incident along the direction normal to the sample surface and a scattering angle of 165 $^\circ$ . In this work, a standard sample consisting on Bi implanted in Si layer with  $N_{\text{SIBi}} = 5.6 \times 10^{15}$  at  $\text{cm}^{-2}$  is used as a reference in order to calibrate the detector channel and the ion energy, as well as to determine the solid angle of the detector. The chemical composition of the films was determined through the simulation of the corresponding RBS spectrum using the SIMNRA program.

**Ellipsometry:** The thickness and the refractive index at 632 nm wavelength were deduced from spectroscopic ellipsometry experiments. The uncertainty of thickness is  $\pm 10$  nm and for the refractive index  $\pm 0.01$ .

**Photoluminescence Spectra:** All the PL spectra of this study were performed at room temperature (RT). Two techniques were used to obtain these spectra. Continuous PL spectra were obtained using the 488 nm excitation wavelength from an  $\text{Ar}^+$  laser with a power of 270 mW on the sample and a chopping frequency of 60 Hz. The spot size of the laser beam was measured by a "moving knife-edge" method and was found to be around 1 mm at  $1/e^2$  of the maximum intensity. For UV excitation at a 239 nm excitation wavelength, time-integrated PL spectra were carried out using an optical parametric oscillator (OPO) having a pulse of 5 ns at full width at half maximum and a repetition rate of 10 Hz. The focusing beam was 500  $\mu\text{m}$  at  $1/e^2$  of the maximum intensity with an average energy of 15 mJ. For these two techniques, a 1 m single grating monochromator (Jobin Yvon) and a liquid-nitrogen-cooled germanium detector (Hamamatsu-R5509-73) were used. These measurements were made by using the standard lock-in techniques (SP830 DPS). All the PL spectra were corrected for the response of the experimental setup and systematically normalized to the film thickness. In order to carefully compare the PL intensities between each sample, a mechanical system was built to place each sample in the same focusing plan of the collected PL.

**Time-resolved Photoluminescence:** The decay times were carried out by means of the OPO at 239 nm excitation wavelength at RT and in using the same experimental set up of the PL spectra. The decay times' data were acquired by a Labview system and an oscilloscope.

**Photoluminescence Excitation:** A 450 W Xenon arc lamp as excitation source was used to carry out the PLE measurements at RT with help of Jobin-Yvon Fluorolog spectrophotometer. All the PLE spectra were corrected by the response of the experimental setup.

## Supporting Information

This work is supported by the CEA/DSM/ENERGY contract (Project HOFELI) and the Chinese Scholarship Council (CSC) program.

## Acknowledgements

The authors would like to thank Dr. Ian Vickridge from SAFIR, “Institut des NanoSciences de Paris” for the RBS data, Dr. Sophie Boudin from CRISMAT Lab for her technical support on the PLE spectra, and Dr. Sébastien Cuffe from the “School of Engineering” (Providence, USA) for his careful re-reading.

- [1] B. S. Richards, *Sol. Energ. Mat. Sol. C.* **2006**, *90*, 2329.
- [2] C. Strümpel, M. McCann, G. Beaucarne, V. Arkhipov, A. Slaoui, V. Svrcek, C. del Canizo, I. Tobias, *Sol. Energ. Mat. Sol. C.* **2007**, *91*, 238.
- [3] Q. Y. Zhang, X. Y. Huang, *Prog. Mater. Sci.* **2010**, *55*, 353.
- [4] D. L. Dexter, *Phys. Rev.* **1957**, *108*, 630.
- [5] a) J. L. Sommerdijk, A. Bril, A. W. de Jager, *J. Lumin.* **1974**, *8*, 341; b) W. W. Piper, J. A. DeLuca, F. S. Ham, *J. Lumin.* **1974**, *8*, 344; c) R. Pappalardo, *J. Lumin.* **1976**, *14*, 159; d) R. T. Wegh, H. Donker, A. Meijerink, R. J. Lamminmäki, J. Hölsä, *Phys. Rev. B* **1997**, *56*, 13841.
- [6] R. T. Wegh, H. Donker, K. D. Oskam, A. Meijerink, *Science* **1999**, *283*, 663.
- [7] T. Trupke, M. A. Green, P. Würfel, *J. Appl. Phys.* **2002**, *92*, 1668.
- [8] K. D. Oskam, R. T. Wegh, H. Donker, E. V. D. van Loef, A. Meijerink, *J. Alloys Compd.* **2000**, *300–301*, 421.
- [9] R. T. Wegh, E. V. D. van Loef, A. Meijerink, *J. Lumin.* **2000**, *90*, 111.
- [10] W. G. J. H. M. van Sark, A. Meijerink, R. E. I. Schropp in *Solar Spectrum Conversion for Photovoltaics Using Nanoparticles, Third Generation Photovoltaics* (Ed: V. Fthenakis), InTech Europe, Croatia **2012**.
- [11] P. Vergeer, T. J. H. Vlugt, M. H. F. Kox, M. I. den Hertog, J. P. J. M. van der Eerden, A. Meijerink, *Phys. Rev. B* **2005**, *71*, 014119.
- [12] Q. Y. Zhang, C. H. Yang, Y. X. Pan, *App. Phys. Lett.* **2007**, *90*, 021107.
- [13] Y. Wang, L. Xie, H. Zhang, *J. Appl. Phys.* **2009**, *105*, 023528.
- [14] G. Alombert-Goget, C. Armellini, S. Berneschi, A. Chiappini, A. Chiasera, M. Ferrari, S. Guddala, E. Moser, S. Pelli, D. N. Rao, G. C. Righini, *Opt. Mater.* **2010**, *33*, 227.
- [15] Q. Duan, F. Qin, D. Wang, W. Xu, J. Cheng, Z. Zhang, W. Cao, *J. Appl. Phys.* **2011**, *110*, 113503.
- [16] G. Lakshminarayana, J. Qiu, *J. Alloys Compd.* **2009**, *481*, 582.
- [17] D. Chen, Y. Wang, Y. Yu, P. Huang, F. Weng, *J. Appl. Phys.* **2008**, *104*, 116105.
- [18] D. Serrano, A. Braud, J.-L. Doualan, P. Camy, R. Moncorgé, *J. Opt. Soc. Am. B* **2011**, *28*, 1760.
- [19] V. D. Rodriguez, V. K. Tikhomirov, J. Méndez-Ramos, A. C. Yanes, V. V. Moshchalkov, *Sol. Energ. Mat. Sol. C.* **2010**, *94*, 1612.
- [20] J. J. Eilers, D. Biner, J. T. van Wijngaarden, K. Kramer, H. U. Gudel, A. Meijerink, *App. Phys. Lett.* **2010**, *96*, 151106.
- [21] X. Y. Huang, Q. Y. Zhang, *J. Appl. Phys.* **2009**, *105*, 053521.
- [22] D. Timmerman, I. Izeddin, P. Stallinga, I. N. Yassievich, T. Gregorkiewicz, *Nat. Photonics* **2008**, *2*, 105.
- [23] N. N. Ha, S. Cuffe, K. Dohnalova, M. T. Trinh, C. Labbé, R. Rizk, I. N. Yassievich, T. Gregorkiewicz, *Phys. Rev. B* **2011**, *84*, 241308(R).
- [24] Y.-T. An, C. Labbé, M. Morales, P. Marie, F. Gourbilleau, *Phys. Stat. Solidi C* **2012**, *9*, 2207.
- [25] S. Cuffe, C. Labbé, L. Khomenkova, O. Jambois, P. Pellegrino, B. Garrido, C. Frilay, R. Rizk, *Mater. Sci. Eng. B* **2012**, *177*, 725.
- [26] J. Kistner, X. Chen, Y. Weng, H. P. Strunk, M. B. Schubert, J. H. Werner, *J. Appl. Phys.* **2011**, *110*, 023520.
- [27] H. Jeong, S.-Y. Seo, J. H. Shin, *App. Phys. Lett.* **2006**, *88*, 161910.
- [28] F. Auzel, *Chem. Rev.* **2004**, *104*, 139.
- [29] Q. Y. Zhang, C. H. Yang, Z. H. Jiang, X. H. Ji, *App. Phys. Lett.* **2007**, *90*, 061914.
- [30] A. Bensalah, M. Ito, Y. Guyot, C. Goutaudier, A. Jouini, A. Brenier, H. Sato, T. Fukuda, G. Boulon, *J. Lumin.* **2007**, *122–123*, 444.
- [31] S. Cuffe, C. Labbé, O. Jambois, B. Garrido, X. Portier, R. Rizk, *Nanoscale Res. Lett.* **2011**, *6*, 395.
- [32] P. Dorenbos, *J. Phys.: Condens. Matter.* **2003**, *15*, 8417.
- [33] H. Kato, N. Kashio, Y. Ohki, K. S. Seol, T. Noma, *J. Appl. Phys.* **2003**, *93*, 239.
- [34] L. Zhang, H. Jin, W. Yang, Z. Xie, H. Miao, L. An, *App. Phys. Lett.* **2005**, *86*, 061908.
- [35] Z. Yuan, D. Li, M. Wang, P. Chen, D. Gong, L. Wang, D. Yang, *J. Appl. Phys.* **2006**, *100*, 083106.
- [36] M. Wang, M. Xie, L. Ferraioli, Z. Yuan, D. Li, D. Yang, L. Pavesi, *J. Appl. Phys.* **2008**, *104*, 083504.
- [37] S. Yerci, R. Li, S. O. Kucheyev, T. van Buuren, S. N. Basu, N. Soumendra, L. D. Negro, *IEEE J. Sel. Topics Quantum Electron.* **2010**, *16*, 114.
- [38] M. Shah, M. Wojdak, A. J. Kenyon, M. P. Halsall, H. Li, I. Crowe, *J. Lumin.* **2012**, *132*, 3103.
- [39] J. C. Vial, A. Bsiesy, F. Gaspard, R. Hérino, M. Ligeon, F. Muller, R. Romestain, R. M. Macfarlane, *Phys. Rev. B* **1992**, *45*, 14171.
- [40] a) I. A. A. Terra, L. J. Borrero-González, T. R. Figueredo, J. M. P. Almeida, A. C. Hernandez, L. A. O. Nunes, O. L. Malta, *J. Lumin.* **2012**, *132*, 1678; b) P. Molina, V. Vasyliov, E. G. Villora, K. Shimamura, *J. Appl. Phys.* **2011**, *110*, 123527; c) S. Ye, B. Zhu, J. Chen, J. Luo, J. R. Qiu, *App. Phys. Lett.* **2008**, *92*, 141112.
- [41] D. J. Robbins, B. Cockayne, B. Lent, J. L. Gasper, *Solid State Commun.* **1976**, *20*, 673.
- [42] a) N. Duhamel-Henry, J. L. Adam, B. Jacquier, C. Linares, *Opt. Mater.* **1996**, *5*, 197; b) F. Auzel, J. Dexpert-Ghys, C. Gautier, *J. Lumin.* **1982**, *27*, 1.
- [43] a) M. A. Green, *Prog. Photovolt.: Res. Appl.* **2012**, *20*, 954; b) W. Shockley, H. J. Queisser, *J. Appl. Phys.* **1961**, *32*, 510.
- [44] a) J. P. Weber, S. Wang, *IEEE J. Quantum Electron.* **1991**, *27*, 2256; b) H. Benisty, R. Stanley, M. Mayer, *J. Opt. Soc. Am. A* **1998**, *15*, 1192;
- [45] A. R. Forouhi, I. Bloomer, *Phys. Rev. B* **1988**, *38*, 1865.
- [46] Z. R. Abrams, A. Niv, X. Zhang, *J. Appl. Phys.* **2011**, *109*, 114905.
- [47] W. R. Taube, A. Kumar, R. Saravanan, P. B. Agarwal, P. Kothari, B. C. Joshi, D. Kumar, *Sol. Energ. Mat. Sol. C.* **2012**, *101*, 32.